Real-time probabilistic seismic hazard assessment based on seismicity anomaly

Yu-Sheng Sun[1*], Hsien-Chi Li[1], Ling-Yun Chang[1], Zheng-Kai Ye[1], and Chien-Chih Chen[1, 2]

[1]Department of Earth Sciences, National Central University, Taoyuan City 32001, Taiwan, R.O.C.

[2]Earthquake-Disaster and Risk Evaluation and Management Center, National Central University, Taoyuan City 32001, Taiwan, R.O.C.

Correspondence: Yu-Sheng Sun (sheng6010@gmail.com)

Abstract

The real-time Probabilistic Seismic Hazard Assessment (PSHA) is developed for considering the practicability for daily life and the rate of seismic activity with time. The real-time PSHA follows the traditional PSHA framework, but the statistic occurrence rate is substituted by time-dependent seismic source probability. Pattern Informatics method (PI) is a proper time-dependent probability model of seismic source, which have been developed over a decade. Therefore, in this research, we chose the PI method as the function of time-dependent seismic source probability and selected two big earthquakes in Taiwan, the 2016/02/05, Meinong earthquake (M_L 6.6) and the 2018/02/06, Hualien earthquake (M_L 6.2), as examples for the real-time PSHA. The forecasting seismic intensity maps produced by the real-time PSHA present the maximum seismic intensity for the

next 90 days. Compared to real ground motion data from the P-alert network, these forecasting seismic intensity maps have considerable effectiveness in forecasting. It indicates that the real-time PSHA is practicable and can provide a useful information for the prevention of earthquake disasters.

1 Introduction

At present, there are two major phases about the researches and applications of seismic hazard: the pre-earthquake and the post-earthquake. The most important usage of the post-earthquake seismic hazard assessment is the Earthquake Early Warning (EEW) system (Cooper, 1868; Wu et al., 1998; Wu et al., 2013). It provides extra time for people to take refuge before the larger seismic wave arrives. On the other hand, Probabilistic Seismic Hazard Analysis (PSHA; Cornell, 1968; SSHAC, 1997) is the most common methodology of the pre-earthquake seismic hazard assessment and mainly for engineering design. PSHA determines the exceeding probability of ground motion level over a specified time period based on the occurrence rate of earthquake and ground motion prediction equations (GMPEs). The occurrence rate of earthquake is generally described by the truncated exponential model (Cosentino et al., 1977) and the characteristic earthquake model (Schwartz and Coppersmith, 1984; Wang et al., 2016). No matter the data is from long-term observations or paleoseismic studies, the earthquake occurrence rate computed from these models will not change with time. However, the seismic activity is a complex dynamic process in time and space and usually fluctuates enormously in short time scale (Chen et al., 2006). Furthermore, the assessment is usually computed by using very long recurrence interval, 475 or 2475 years, for the purpose of engineering design (Iervolino et al., 2011). As a result, it is hard to verify the accuracy of seismic hazard assessment in limited life because of such long period. On the other hand, such long interval is suitable for buildings, but not for human's life which is definitely much shorter than the life span of buildings. In other words, the concept of catastrophic in such long recurrence intervals is difficult to resonate in the daily life of general public. In addition, the definition like 10% probability in 50 years is hard to image for most ordinary people. Therefore, a statistical long-term seismic hazard assessment is useless in our daily life. On the contrary, we believe that a short-term and time-dependent pre-earthquake hazard assessment is necessary for everyone's daily use. In this study, we suggested a preliminary method to achieve this goal by using a time-dependent seismic source probability instead of the static one in the long-term assessment. One of the capable candidates as a time-dependent seismic source probability is the Pattern Informatics (PI) method, which has developed over the past decade (Rundle et al., 2000; Tiampo et al., 2002; Wu et al., 2008a; Chang et al., 2016).

Anomalous change in seismicity is widely used as precursory indicator for big earthquakes and is usually classified into seismic activation or seismic quiescence, depending on ascending or descending number or occurrence rate of seismicity (Chen et al., 2005; Wu et al., 2008b). In the PI method, big earthquakes tend to occur after precursory anomalous seismic changes and its occurrence probability can be quantified by the magnitude of spatiotemporal variation of seismicity. In preliminary researches, PI performs good in identifying locations nearby upcoming big earthquakes. A modified version of PI developed in the recent researches has obviously improved the accuracy of identifying occurrence time interval of big earthquakes. The occurrence probability of big earthquakes in the next 90 days is plausible after a series of verification (Chang et al., 2016; Chang, 2018). Therefore, we used the modified PI method to compute the time-dependent seismic source probability of each location while the area of interest is coarse-grained by square in uniform size.

In this research, we illustrate a simple way to achieve a real-time seismic hazard assessment. The crucial step is to replace statistical seismic probability by the time-dependent probability from the modified PI method. The real-time seismic hazard assessment produced the seismic hazard forecasting maps for the next 90 days. The “real-time” PSHA can be updated with earthquake catalog refreshing (time-dependent) and forecast for the near future (short-term), and compared with the forecasting time scale and static seismic rate of the traditional PSHA, these can be called "real-time". We illustrated this real-time assessment process by two recent big earthquakes in Taiwan, the 2016 Meinong earthquake (M_L 6.6) (Lee et al., 2016; Chen et al., 2017; Lee et al., 2017) and the 2018 Hualien earthquake (M_L 6.2) (Hsu et al., 2018). Detailed parameters about these two earthquakes are listed in Table 1. Finally, the reliability of the seismic hazard maps was verified by comparing with real ground motion data recorded by the P-alert network.

2 Data

2.1 Central Weather Bureau Seismic Network (CWBSN) catalog

We used the CWBSN catalog maintained by the Central Weather Bureau (CWB), Taiwan (https://www.cwb.gov.tw/V7e/earthquake/seismic.htm and http://gdms.cwb.gov.tw/index.php, last access: July 2018). The completeness magnitude (M_c) of this catalog is estimated approximately 2.0 in local magnitude (M_L) (Wu et al., 2008c). In the analysis of focal depth, Wu et al. (2008b) showed that the focal depth for about 80% earthquakes is shallower than 30 km. Therefore, we used M_L 2.0 and 30 km as the threshold of magnitude and focal depth to select earthquakes used in the PI calculation.

2.2 P-alert network

In this research, the ground motion recordings from the P-alert network were used to verify the effectiveness of the real-time seismic hazard assessments from our idea. The EEW research group of the National Taiwan University (NTU) have begun to set up the P-alert real-time strong-motion network since 2010. The device of the P-alert network can record real-time acceleration signals in three-component and publish alerts if the peak initial-displacement amplitude (*Pd*) or peak ground acceleration (PGA) exceeds a redefined threshold (Wu et al., 2013, 2016b). Nowadays, there are more than 600 stations in Taiwan; most of them are located in elementary schools (Wu et al., 2013; Yang et al., 2018). We mainly adopted the P-alert waveform database maintained by Taiwan Earthquake research Center (TEC) and the data from NTU were as an auxiliary catalog (The data of the P-alert network can be downloaded from the Data Center of TEC: http://palert.earth.sinica.edu.tw/db/ (last access: July 2018) or contact with Prof. Yih-Min Wu at NTU for NTU's catalog: drymwu@ntu.edu.tw). However, even if there are so many stations covering Taiwan, the distribution of the P-alert network is still nonuniform (see Fig. 2b and 3b). This nonuniform distribution may causes some problems that we will discuss later.

3 Method

3.1 Pattern Informatics (PI)

The physical fundamental of the PI method is phase dynamics which describes changes of a system by rotation of state vector in the Hilbert space (Rundle et al., 2002; 2003). The evolution of state vector in a dynamic fault system is suggested to be related to stress accumulation and release (Chen et al., 2006). The computation steps we addressed here are a modified version developed by Chang et al. (2016) and Chang (2018) to improve temporal resolution of the PI. The research area (119°~123° E 21°~26° N) is divided into boxes of grid size 0.1°×0.1°, and each box is indicated by parameter x_i. Because of the M_c and the distribution of focal depth (mentioned in Section 2.1), all events having $M_L \geq 2.0$ and depth ≤ 30 km were used. In the PI computation, t_1 and t_2 are the beginning and the end of a change interval, respectively, and the length of a change interval is 4 years. The beginning time of calculation, t_0, is defined as 12 years before t_2. Then, t_b is a sampling reference time between t_0 and t_1. The t_b starts from t_0 and shifts forward 3 days in each calculation until the length of time between t_b and t_1 being a half change interval. The forecasting interval, t_3, starts after t_2 (Chang, 2018). The seismicity rate in the time period t_b to t (t_b to t_1 and t_b to t_2) can be expressed as

$$S(x_i, t_b, t) = \frac{1}{t - t_b} \int_{t_b}^{t} n(x_i, t) dt \qquad (1)$$

In this study, we conservatively consider the earthquake number, n, occurring in the x_i and its eight neighboring boxes. The rate change during the change interval can be expressed as

$$\Delta S(x_i, t_b, t_1, t_2) = S(x_i, t_b, t_2) - S(x_i, t_b, t_1) \qquad (2)$$

$S(x_i, t_b, t)$ is a vector in a Hilbert space that records present seismic activity, so ΔS can be interpreted as an angular drift of S (Rundle et al., 2002; Tiampo 2002). To reduce the time-dependent background seismicity, we take temporal standard score normalizing ΔS, and obtain $\Delta\tilde{S}$. To compare the high and low levels of seismicity rate change in each grid box at the same t_b, we then take spatial standard score normalizing $\Delta\tilde{S}$, and obtain $\Delta\hat{S}$. The average of the absolute value at all t_b points in each x_i is

$$\Delta s(x_i) = \frac{1}{|\{t_b\}|}\sum_{t_b=t_0}^{t_b}\left|\Delta\hat{S}(x_i, t_b, t_1, t_2)\right| \tag{3}$$

Then, the mean squared change in probability

$$\Delta P(x_i) = \Delta s^2(x_i)$$

is computed (Chen et al., 2005; Chang et al., 2016). In this study, we further divide the magnitude range of earthquakes into several segments to separately calculate the relative probabilities $\Delta P(x_i)$. The divided magnitude range is from magnitude of 2.0 with window length 0.5, and it shifts forward by 0.2 each time. Then, we calculate relative probability each time, such as $\Delta P(x_i)_{2.0\sim2.5}$, $\Delta P(x_i)_{2.2\sim2.7}$. Finally, we multiply all of the relative probabilities.

$$\Delta P_M = \prod \Delta P_{i\sim i+0.5} \tag{4}$$

ΔP_M to forecast earthquakes is referred to as the modified pattern informatics method (Chang, 2018). According to Chang et al. (2016), the forecasting interval of the PI method reaches 90 days. Lastly, the PI method produces a forecasting probability distribution of seismic sources for $M_L \geq 5.0$ within the forecasting interval.

3.2 Real-time PSHA

In the traditional PSHA framework (Cornell, 1968; Wang et al., 2016), the probability of an earthquake's occurrence follows the Poisson process and the average recurrence interval for an annual frequency of exceedance can be expressed as

$$v(Z > z) = \sum_{i=1}^{N_s} \dot{N}_i \iint f_{M_i}(m)\, f_{R_i}(r)\, P(Z > z \mid m, r)\, dm\, dr \tag{5}$$

where $f_{M_i}(m)$ and $f_{R_i}(r)$ are the probability density functions of magnitude and distance, respectively; $P(Z > z \mid m, r)$ is the conditional probability of ground motion Z exceeding a specified value z for a specific magnitude m and distance r. $\dot{N}_i$ is the annual occurrence rate of earthquakes and described by the truncated exponential model (Cosentino et al., 1977) and the characteristic earthquake model (Schwartz and Coppersmith, 1984). Finally, to consider all scenarios, the total probability of N_s earthquakes is summarized in a given region.

In the real-time PSHA, the occurrence rate of earthquake used in the traditional PSHA framework is replaced by seismic forecasting probability to achieve spatiotemporal variability of the hazard assessment. Then, considering the gridded space, the real-time PSHA can be expressed as

$$v(Z > z) = \sum^{M_s} \sum^{Loc_s} P_{M_i, Loc_i}(m, loc)\, P(Z > z | m, loc) \tag{6}$$

where $P_{M_i\,,\,Loc_i}(m, loc)$, the forecasting probability distribution, is a function of magnitude and location. It specifies an occurrence probability for specific magnitude, M_i, at each spatial location, Loc_i. The summations are to consider the whole of the contribution from any possible magnitude, M_s, and location, Loc_s. In this research, we adopted the forecasting probability from the PI method as $P_{M,Loc}(m, loc)$. Loc refers to x_i in the PI method. The forecasting probability of the PI method presents a distribution of cumulative forecasting probability for $M_L \geq 5.0$. Thus, we referred to the average character of Gutenberg-Richter law in Taiwan (Gutenberg and Richter, 1944; Wang et al., 2015) to turn it into probability density function (PDF). It can be corresponded to the specific magnitude conditions for $P(Z > z \mid m, loc)$. To evaluate the ground motion, we used the GMPE published by Lin et al. (2012),

$$\ln y = C_1 + F_1 + C_3(8.5 - M_w)^2 + [C_4 + C_5(M_w - 6.3)] \ln\left\{\sqrt{[R^2 + exp(H)^2]}\right\} + C_6 F_{NM} + C_7 F_{RV} + C_8 \ln\left(\frac{V_s 30}{1130}\right)$$

$$F_1 = C_2(M_w - 6.3), \qquad M_w \leq 6.3$$

$$F_1 = -HC_5(M_w - 6.3), \qquad M_w > 6.3 \tag{7}$$

which was also adopted for the issue of Taiwan PSHA in Lee et al. (2017). In Eq. 7, C_1 to C_8 and H are the regression coefficients (Table 2); R is the closest distance (km); F_{NM} and F_{RV} represent the earthquake type: $F_{NM} = 1$ and $F_{RV} = 0$ for normal fault earthquake; $F_{NM} = 0$ and $F_{RV} = 1$ for reverse fault earthquake. In this GMPE, the earthquake type is one of the important parameters. However, the divisions of seismic source in the PI method is no longer based on the geological classification, but the grid box, x_i. Considering that the most faults in Taiwan are reverse faults (Shyu et al., 2016), we adopted the reverse fault parameters setting for the entire research area. V_s is eclectically assigned $V_s = 760$. Using the conversion equation written in Lin and Lee (2008), which is adopted in Lin (2012), turns M_L into M_w. Finally, the forecasting maximum PGA from the real-time PSHA is transferred to seismic intensity according to the seismic intensity scale of CWB listed in Table 3 (Wu et al., 2003). It means that the forecasting seismic intensity map presents the maximum seismic intensity which every site will encounter in the following 90 days.

3.3 Performance verification

3.3.1 Receiver Operating Characteristic curve (ROC)

The ROC diagram is a binary classification model and widely used as a tool for quantifying the performance of earthquake prediction (Holliday et al., 2006; Nanjo et al., 2006; Wu et al., 2016a). We used the ROC diagram as an objective quantitative indicator to evaluate the performance of the forecasting seismic probability computed by the PI method. For each box x_i, there are four situations, parameters, while comparing forecasting hotspot and target earthquake: a means any target earthquake in a hotspot; b means no target earthquake in a hotspot; c means no hotspot but with at least one target earthquake; d means no target earthquake and no hotspot. True positive rate (TPR) is defined as $a/(a+c)$ and false positive rate (FPR) is defined as $b/(b+d)$. The values of a, b, c, and d change with threshold of forecasting probability, and therefore TPR and FPR change as well. The area under the ROC curve (AUC) is between 0 and 1. AUC=1 is a perfect prediction; AUC=0.5 is a random guess. For each forecasting map of PI, we generated 1000 random tests by re-distributing the hotspots randomly over the research area to examine the possibility that a specific distribution of hotspots can generate by chance. In Fig. 1c and 1d, the blue line is the 95% confidence interval based on two standard deviations. The standard deviation is calculated by the random test results in each bin of the x-axis. The 95% confidence interval helps us differentiate the distributing range of random tests and the significant of forecasting probability.

3.3.2 Average Percent Hit Rate (APHR)

The success rate of forecasting seismic intensity is a predictive accuracy of classification problems for which the average percent hit rate (APHR) is arguably the most intuitive measure of discrimination. The APHR is a rate at which the forecasting data are classified into the correct classes (Sharda and Delen, 2006). In this research, the APHR was used to quantify the forecasting performance of the real-time seismic hazard assessments. In the APHR, the exact hit rate which only counts the correct classifications to the exact same class can be expressed as:

$$\mathrm{APHR}_{\mathrm{exact}} = \frac{1}{N}\sum_{i=1}^{g} p_i \qquad (8)$$

where, in our case, N is the total number of the P-alert stations or the boxes on the forecasting hazard map, g is the total number of seismic intensity classes (=8, according to the CWB's seismic intensity scale), and p_i is the total number of samples classified as class i. In the random test, we further generated 1000 random tests by randomly re-distributing the forecasting maximum seismic intensity over the research area and the stations to examine the possibility that a specific distribution of the forecast can generate by chance.

4 Results

4.1 Forecast of earthquake occurrences

Figure 1a and 1b show the forecasting probability maps computed by the PI method, and Fig. 1c and 1d are corresponding forecasting performance verified by the ROC tests. In the case of 2016 Meinong earthquake, t_0, t_1, and t_2 are 2004/01/31, 2012/01/31, and 2016/01/31. In the case of 2018 Hualien earthquake, t_0, t_1, and t_2 are 2006/01/31, 2014/01/31, and 2018/01/31. The forecasting intervals of both cases are 90 days after t_2. Cyan star in Fig. 1a and 1b is the main shock of 2016 Meinong and 2018 Hualian earthquakes, and the biggest earthquake in the forecasting interval. Gray circles in Fig. 1a and 1b are the earthquakes with magnitude $M_L \geq 5.0$ in the forecasting interval, and more detailed information about these earthquakes can be obtained in Table 1. A notable point is that both main shocks and most big earthquakes are located in or very close to the hotspots. The performance of the PI forecasting probabilities seems to be good simply by visual inspection.

In Fig. 1c and 1d, red curves are far above the blue curves (95% confidence interval). The AUCs of red curves are 0.91 and 0.94, and are apparently larger than the AUCs of blue curves, which are 0.73 and 0.70. The ROC tests verified quantitatively that the performance of the PI forecasting probability is significant, and these patterns are not just generated by random distribution of hotspots by chance. Both distributions of hotspot are physically meaningful. Therefore, we can use these probability maps as the function of earthquake occurrence rate in subsequent calculation for the real-time PSHA.

4.2 Real-time PSHA

In Fig. 2 and 3, panel (a) shows the map of forecasting max seismic intensity estimated by the real-time PSHA for the forecasting interval; panel (b) shows the map of max seismic intensity recorded by the P-alert network during the forecasting interval. To ensure that it is absolutely maximum intensity during the forecasting interval, we only used the stations which have recorded all the target events ($M_L \geq 5.0$) in the forecasting interval. Although there are over 600 P-alert stations distributing widely in Taiwan, some boxes still do not contain any station, for example, the Central Mountain Range (see Fig. 5a and 5b). Therefore, we had to estimate the intensities in such kind of boxes by interpolating. Thus, this strategy indeed generates the artificial effect and we will show it later.

Comparing Fig. 2a and 2b, we suggest that both seismic intensity distributions are very similar. An apparent deviation of forecasting seismic intensities from the recorded values is in the southwestern Taiwan, especially the area closer to the 2016 Meinong main shock. Fig. 2c shows the difference of intensity between Fig. 2a and 2b; the color of blue and red means that the forecasting value in a box is underestimated or overestimated. Most boxes have intensity difference in the range -1 to 1, but some boxes in the southwestern Taiwan are underestimated; the differences are most 2 or even up to 3.

Comparing Fig. 3a and 3b, we suggest that both seismic intensity distributions are still very similar. In this case, an apparent deviation of forecasting seismic intensities from the recorded values is in the southern Taiwan and a part of southwestern area. Figure 3c shows that most boxes in the southern Taiwan have smaller recorded intensity, and the recorded intensities in a part of southwestern Taiwan are larger than the forecasting values.

Figure 4 shows the verifications generated by the APHR to quantitatively evaluate the performance of the forecasting seismic intensity. We considered the denominator of two classifications in Eq. 8, i.e. the total number of the P-alert stations and the total number of boxes in the research area. The results are indicated by "P-alert" and "Map" in Fig. 4, respectively. While comparing forecasting intensity to recorded value, both cases "forecasting = recorded" and "forecasting = recorded +1" belong to "successful forecasting". The definition of the tolerance range that depends on the perspectives and allowance of different users is certainly debatable (Hsu et al., 2018). In our case, the reason is that considering to prevent or mitigate earthquake disaster, “overestimation” is better than “underestimation”. Therefore, we tolerated the case of overestimation of 1 intensity rather than underestimation.

First, all red lines are above the maximum hit rate of random tests and higher than 0.5, not to mention the random guess of the eight choices of the seismic intensity scale. It means that these forecasting seismic intensity maps have considerable effectiveness in the forecast, and their good performance can’t merely happen by chance. Moreover, another property is that both hit rates of the “P-alert” cases are higher than the rates of the “map” cases. This result could be attributed to the influence of the artificial effect generated by the interpolation of seismic intensity from the P-alert data of nonuniform distribution. Last, it is emphasized that we just focus on the earthquakes with $M_L \geq 5$ in this research, but we cannot deny the possibility of a $M_L < 5$ earthquake to cause large seismic intensity in the near field.

5 Discussion

The results of the APHR performance test indicates that the maps and stations of forecasting max seismic intensity by the real-time PSHA are significant and effective. Figure 5 is a concretization of the APHR verification and further gives more details. It clearly shows the P-alert station distributions of the "hit" and "not hit", considering only the station-to-station prediction relationship between the forecasts and records. In both cases, most of the P-alert stations are hit (Fig. 5a and 5b), and the hit percentages distribute along the diagonal and tolerant ranges (Fig. 5c and 5d). However, there still are some locations or stations with wrong forecast. In the case of 2016 Meinong earthquake, the stations located in the southwestern Taiwan do not match the real records, and at high seismic intensities (>3), the forecasting results at some stations are underestimated (Fig. 5c), especially in the southwestern area. In the case of 2018 Hualien earthquake, the result from the "P-alert" APHR seems better than former, and further the distribution of the hit percentage is more concentrated along the diagonal and tolerant ranges. Nevertheless, the stations in the southern and part of southwestern Taiwan are still missed. These abovementioned differences between forecasting results and recorded seismic intensities in both cases can be mainly attributed to three aspects.

First of all, the forecasting model that determines the probability distributions of earthquake occurrences is critical for the real-time PSHA. If the probability distribution is missing or false alarm in somewhere, it directly causes the inaccurate forecasts to the real-time PSHA. In the PI results, some differences are located on the hotspots with relatively higher probability, for example, the area in 22.6º to 23ºN and 120.9º to 121.3ºE in Fig. 1a, and 22.7º to 23.1ºN and 120.4º to 120.8ºE in Fig. 1b. Compared the locations of the earthquakes, these hotspots just shift slightly and it seems acceptable. However, in the results of the real-time PSHA, it leads the maps of forecasting max seismic intensity to underestimate in the area near the epicenters and overestimate in the area without any earthquake event, but with high probability of earthquake occurrence. For instance, the southwestern area in the case of 2018 Hualien earthquake is underestimated because of this reason, and then it also causes overestimated in the southern area (see Fig. 3 and 5b). Therefore, a more accurate and precise forecasting model helps us get a more positive result in a real-time PSHA. Even if the PI results perform well in the ROC test, the PI method still needs to be improved.

Secondly, the evaluation of earthquake ground motion suffers from the limitations of GMPEs. We adopted the GMPE produced by Lin et al. (2012) whose data ($M_L \geq 5.0$) within 50 km are less than 14% of all data for the regression of GMPE. If there is a shortage of data in near field and for larger events in the regression of GMPEs, the applicability of GMPEs is limited (Edwards and Fäh, 2014). Therefore, that probably causes the deviation of evaluation on forecasting seismic intensity maps, for instance, the underestimation of the areas around the two main shocks (Fig. 2c and 3c). Moreover, the site effect is difficult to be properly and comprehensively evaluated in GMPEs, but it dramatically affects the behavior of seismic waves. For example, the amplitudes in the Meinong earthquake were amplified extending along the northwest (in Fig. 2b) because of the Western Plain composed of thick and low velocity sedimentary deposits (see Fig. 4 in Lee et al., 2016). As a result, the site effect also contributes and leads the seismic intensity forecast to underestimate (Fig. 2c and 5a).

Last but not least, the directivity effect also plays an important role in the distribution of ground motion. For the main shocks in two cases, the rupture characteristic brings a strong directivity effect that causes the significant amplification of ground motion along the rupture direction (Lee et al., 2016; Hsu et al., 2018). However, GMPEs are basically a statistical distribution of PGA generated by all data at the same radical distance without considering possible effect of rupture directivity. As a result, GMPEs are only able to provide the ground motion estimation of radial extension. Besides, the forecasting model does not include the information of rupture direction either. Therefore, we suggest that some differences which along the rupture direction may belong to this effect.

6 Conclusion

This study presents how the real-time seismic hazard assessment can be achieved by replacing the static seismic rate, i.e. the truncated and characteristic earthquake models, with the time-dependent seismic source probability of the PI method. With regard to the time-dependent seismic source probability, the ROC tests verified quantitatively that the performances of the PI forecasting probabilities in forecasting interval are quite effective. Therefore, those significant probability distributions can be used as the function of earthquake occurrence rate, $P(m, loc)$, in the real-time PSHA. Our forecasting seismic intensity maps of the real-time PSHA have the hit rates outperformed the random guesses and higher than 0.5 for both cases of the Meinong and Hualien earthquakes. This study thus suggests that these real-time PSHA maps are effective in terms of forecasting, and their good performances are not likely coincidence. We demonstrated that the real-time seismic hazard assessment is doable and can be realized and updated by the time-dependent seismic source probability.

In the future, the different time-dependent seismic source probability models can be introduced to provide a more accurate and robust estimation for earthquake occurrences. Also, a possible improvement for our results could be from the estimated PGA distribution not only by means of the state-of-the-art machine learning tools for a big data bank of the P-alert network but also by physics-based numerical simulations (PBS) of seismic ground motion, instead of the empirical GMPEs. Presumably, a real-time forecasting map of seismic intensity enables governments or businesses to efficiently prepare for earthquake disasters. Moreover, the seismicity intensity scale based on PGA are related to the vulnerability level of buildings, which will also be changed with time due to the degradation and upgrades (e.g. obsolescence, retrofitting actions, climate events). Therefore, when further assessing a seismic risk fluctuating with time, the real-time PSHA and the change of vulnerability should be considered.

Acknowledgments

The authors are grateful for research support from the Ministry of Science and Technology (ROC) and the Department of Earth Science, National Central University, Taiwan (ROC). This work is supported by "Earthquake-Disaster & Risk Evaluation and Management Center, E-DREaM" from The Featured Areas Research Center Program within the framework of the Higher Education Sprout Project by the Ministry of Education (MOE) in Taiwan.

References

Chang, L.-Y., Chen, C.-c., Wu, Y.-H., Lin, T.-W., Chang, C.-H., and Kan, C.-W.: A Strategy for a Routine Pattern Informatics Operation Applied to Taiwan, Pure Appl. Geophys., 173, 235-244, doi:10.1007/s00024-015-1079-9, 2016.

Chang, L.-Y.: A study on an improved pattern informatics method and the soup-of-group model for earthquakes. Doctoral dissertation, Department of Earth Sciences, National Central

University, Taiwan, R. O. C., 2018.

Chen, C.-c., Rundle, J. B., Holliday, J. R., Nanjo, K. Z., Turcotte, D. L., Li, S.-C., and Tiampo, K. F.: The 1999 Chi-Chi, Taiwan, earthquake as a typical example of seismic activation and quiescence, Geophys. Res. Lett., 32, L22315, doi:10.1029/2005GL023991, 2005.

Chen, C.-c., Rundle, J. B., Li, H.-C., Holliday, J. R., Turcotte, D. L., and Tiampo, K. F.: Critical point theory of earthquakes: Observation of correlated and cooperative behavior on earthquake fault systems, Geophys. Res. Lett., 33, L18302, doi:10.1029/2006GL027323, 2006.

Chen, H.-J., Chen, C.-c., Ouillon, G., and Sornette, D.: Using geoelectric field skewness and kurtosis to forecast the 2016/2/6, M L 6.6 Meinong, Taiwan Earthquake, Terr. Atmos. Ocean. Sci., 28, 745-761, doi:10.3319/TAO.2016.11.01.01, 2017.

Cooper, J. D.: Letter to editor, San Francisco Daily Evening Bulletin, Nov. 3, 1868.

Cornell, C. A.: Engineering seismic risk analysis, Bull. Seismol. Soc. Am., 58, 1583-1606, 1968.

Cosentino, P., Ficarra, V., and Luzio, D.: Truncated exponential frequency-magnitude relationship in earthquake statistics, Bull. Seismol. Soc. Am., 67, 1615-1623, 1977.

Edwards, B., and Fäh, D.: Ground motion prediction equations, ETH-Zürich, 2014.

Holliday, J. R., Rundle, J. B., Turcotte, D. L., Klein, W., Tiampo, K. F., and Donnellan, A.: Space-Time Clustering and Correlations of Major Earthquakes, Phys. Rev. Lett., 97, 238501, doi:10.1103/PhysRevLett.97.238501, 2006.

Gutenberg, B. and Richter, C. F.: Frequency of earthquakes in California, Bull. Seism. Soc. Am., 34, 185–188, 1944.

Hsu, T. Y., Lin, P. Y., Wang, H. H., Chiang, H. W., Chang, Y. W., Kuo, C. H., Lin, C. M., and Wen, K. L.: Comparing the Performance of the NEEWS Earthquake Early Warning System Against the CWB System During the 6 February 2018 Mw 6.2 Hualien Earthquake, Geophys. Res. Lett., 45, 6001-6007, doi:10.1029/2018GL078079, 2018.

Iervolino, I., Chioccarelli, E., and Convertito, V.: Engineering design earthquakes from multimodal hazard disaggregation, Soil Dynam. Earthquake Eng., 31, 1212-1231, https://doi.org/10.1016/j.soildyn.2011.05.001, 2011.

Lee, S.-J., Yeh, T.-Y., and Lin, Y.-Y.: Anomalously Large Ground Motion in the 2016 ML 6.6 Meinong, Taiwan, Earthquake: A Synergy Effect of Source Rupture and Site Amplification, Seismol. Res. Lett., 87, 1319-1326, doi:10.1785/0220160082, 2016.

Lee, Y.-T., Wang, Y.-J., Chan, C.-H., and Ma, K.-F.: The 2016 Meinong earthquake to TEM PSHA2015, Terr. Atmos. Ocean. Sci., 28, 703-713, doi:10.3319/TAO.2016.12.28.02, 2017.

Lin, P.-S., Lee, C.-T.: Ground-Motion Attenuation Relationships for Subduction-Zone Earthquakes in Northeastern Taiwan, Bull. Seism. Soc. Am., 98 (1): 220–240. doi: https://doi.org/10.1785/0120060002, 2008.

Lin, P.-S., Hsie, P.-S., Lee, Y.-R., Cheng, C.-T., and Shao, K.-S.: The research of probabilistic seismic hazard analysis and geological survey of nuclear power plant: Construction of ground motion prediction equation for response spectra., Commission Report of the Institute of Nuclear Energy Research, Atomic Energy Council, Executive Yuan. (in Chinese), 2012.

Nanjo, K. Z., Holliday, J. R., Chen, C.-c., Rundle, J. B., and Turcotte, D. L.: Application of a modified pattern informatics method to forecasting the locations of future large earthquakes in the central Japan, Tectonophysics, 424, 351-366, https://doi.org/10.1016/j.tecto.2006.03.043, 2006.

Rundle, J. B., Klein, W., Tiampo, K., and Gross, S.: Linear pattern dynamics in nonlinear threshold systems, Phys. Rev. E, 61, 2418-2431, doi:10.1103/PhysRevE.61.2418, 2000.

Rundle, J. B., Tiampo, K. F., Klein, W., and Sá Martins, J. S.: Self-organization in leaky threshold systems: The influence of near-mean field dynamics and its implications for earthquakes, neurobiology, and forecasting, Proc. Nat. Acad. Sci., 99, 2514-2521, doi:10.1073/pnas.012581899, 2002.

Rundle, J. B., Turcotte, D. L., Shcherbakov, R., Klein, W., and Sammis, C.: Statistical physics approach to understanding the multiscale dynamics of earthquake fault systems, Rev. Geophys., 41, 1019, doi:10.1029/2003RG000135, 2003.

Senior Seismic Hazard Analysis Committee (SSHAC): Recommendations for probabilistic seismic hazard analysis: guidance on uncertainty and use of experts, US Nuclear Regulatory Commission Washington, DC, 1997.

Schwartz, D. P., and Coppersmith, K. J.: Fault behavior and characteristic earthquakes: Examples from the Wasatch and San Andreas Fault Zones, J. Geophys. Res., 89, 5681-5698, doi:10.1029/JB089iB07p05681, 1984.

Sharda, R., and Delen, D.: Predicting box-office success of motion pictures with neural networks, Expert Syst. Appl., 30, 243-254, https://doi.org/10.1016/j.eswa.2005.07.018, 2006.

Shyu, J. B. H., Chuang, Y.-R., Chen, Y.-L., Lee, Y.-R., and Cheng, C.-T.: A New On-Land Seismogenic Structure Source Database from the Taiwan Earthquake Model (TEM) Project for Seismic Hazard Analysis of Taiwan, Terr. Atmos. Ocean. Sci., 27, 311-323, doi:10.3319/TAO.2015.11.27.02(TEM), 2016.

Tiampo, K. F., Rundle, J. B., McGinnis, S., Gross, S. J., and Klein, W.: Mean-field threshold systems and phase dynamics: An application to earthquake fault systems, Europhys. Lett., 60, 481, doi:10.1209/epl/i2002-00289-y, 2002.

Wang, J.-H., Chen, K.-C., Leu, P.-L., and Chang, J.-H.: b-Values Observations in Taiwan: A Review, Terr. Atmos. Ocean. Sci., 26, 475-492, doi:10.3319/TAO.2015.04.28.01(T), 2015.

Wang, Y.-J., Chan, C.-H., Lee, Y.-T., Ma, K.-F., Shyu, J. B. H., Rau, R.-J., and Cheng, C.-T.: Probabilistic Seismic Hazard Assessment for Taiwan, Terr. Atmos. Ocean. Sci., 27, 325-340, doi:10.3319/TAO.2016.05.03.01, 2016.

Wu, Y.-M., Shin, T.-C., and Tsai, Y.-B.: Quick and reliable determination of magnitude for seismic early warning, Bull. Seismol. Soc. Am., 88, 1254-1259, 1998.

Wu, Y.-M., Teng, T.-l., Shin, T.-C., and Hsiao, N.-C.: Relationship between Peak Ground Acceleration, Peak Ground Velocity, and Intensity in Taiwan, Bull. Seismol. Soc. Am., 93, 386-396, doi:10.1785/0120020097, 2003.

Wu, Y.-H., Chen, C.-c., and Rundle, J. B.: Detecting precursory earthquake migration patterns using the pattern informatics method, Geophys. Res. Lett., 35, L19304, doi:10.1029/2008GL035215, 2008a.

Wu, Y.-H., Chen, C.-c., and Rundle, J. B.: Precursory seismic activation of the Pingtung (Taiwan) offshore doublet earthquakes on 26 December 2006: A pattern informatics analysis, Terr. Atmos. Ocean. Sci., 19, 743-749, doi:10.3319/TAO.2008.19.6.743(PT), 2008b.

Wu, Y.-M., Chang, C.-H., Zhao, L., Teng, T.-L., and Nakamura, M.: A Comprehensive Relocation of Earthquakes in Taiwan from 1991 to 2005, Bull. Seismol. Soc. Am., 98, 1471-1481, doi:10.1785/0120070166, 2008c.

Wu, Y.-M., Chen, D.-Y., Lin, T.-L., Hsieh, C.-Y., Chin, T.-L., Chang, W.-Y., and Li, W.-S.: A High-Density Seismic Network for Earthquake Early Warning in Taiwan Based on Low Cost Sensors, Seismol. Res. Lett., 84, 1048-1054, doi:10.1785/0220130085, 2013.

Wu, Y.-H., Chen, C.-c., and Li, H.-C.: Conditional Probabilities for Large Events Estimated by Small Earthquake Rate, Pure Appl. Geophys., 173, 183-196, doi:10.1007/s00024-014-1019-0, 2016a.

Wu, Y.-M., Liang, W.-T., Mittal, H., Chao, W.-A., Lin, C.-H., Huang, B.-S., and Lin, C.-M.: Performance of a Low-Cost Earthquake Early Warning System (P-Alert) during the 2016 ML 6.4 Meinong (Taiwan) Earthquake, Seismol. Res. Lett., 87, 1050-1059, doi:10.1785/0220160058, 2016b.

Yang, B. M., Huang, T.-C., and Wu, Y.-M.: ShakingAlarm: A Nontraditional Regional Earthquake Early Warning System Based on Time-Dependent Anisotropic Peak Ground-Motion Attenuation Relationships, Bull. Seismol. Soc. Am., 108, 1219-1230, doi:10.1785/0120170105, 2018.

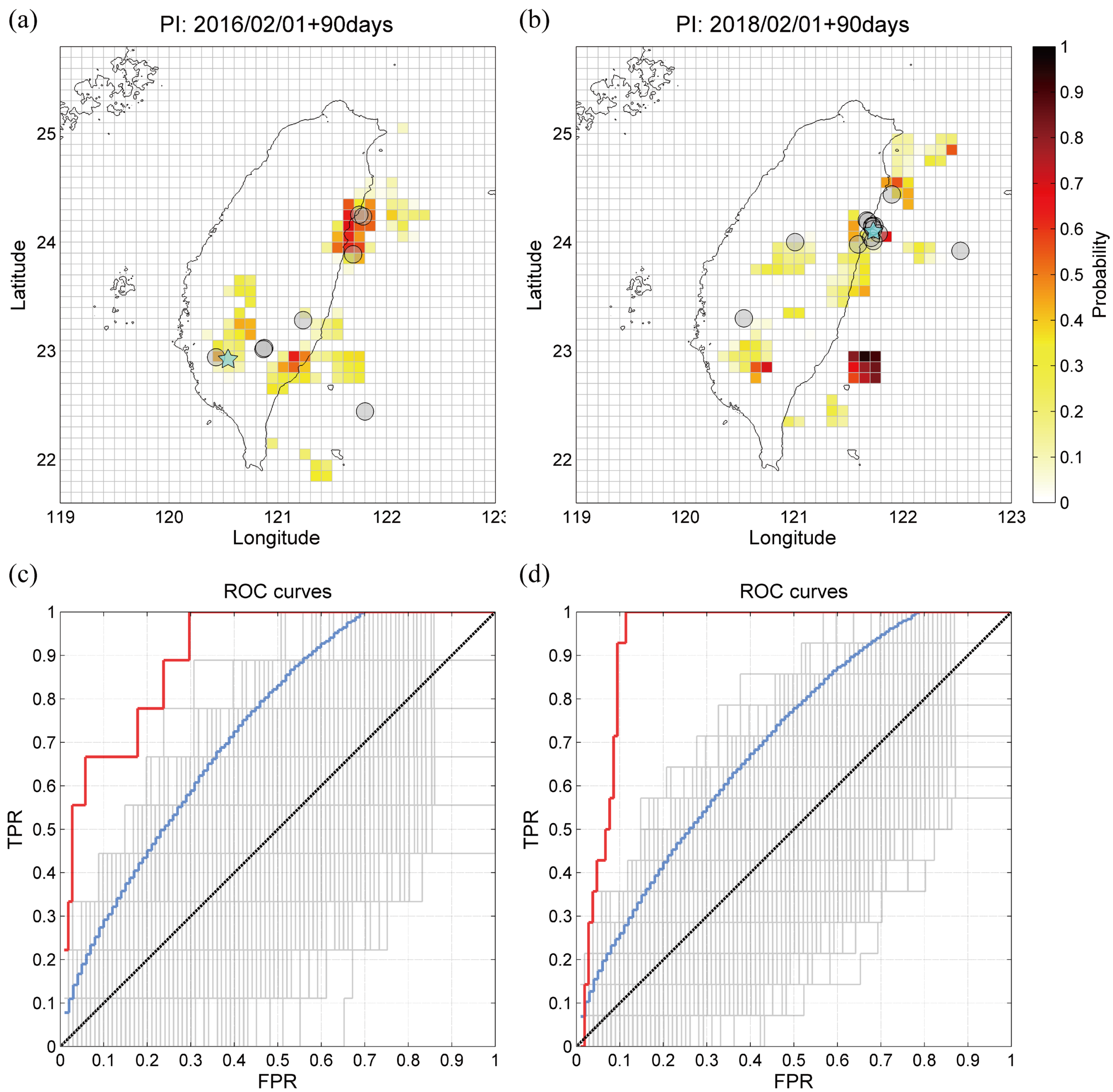

Figure 1. Panels (a) and (b) show the forecasting probability maps of the Meinong earthquake and the Hualien earthquake, respectively. Panels (c) and (d) are the ROC curves of (a) and (b), respectively. Red, gray, blue, and black curve represent the forecasting probability map, random tests, 95% confidence interval, and the average of random tests, respectively.

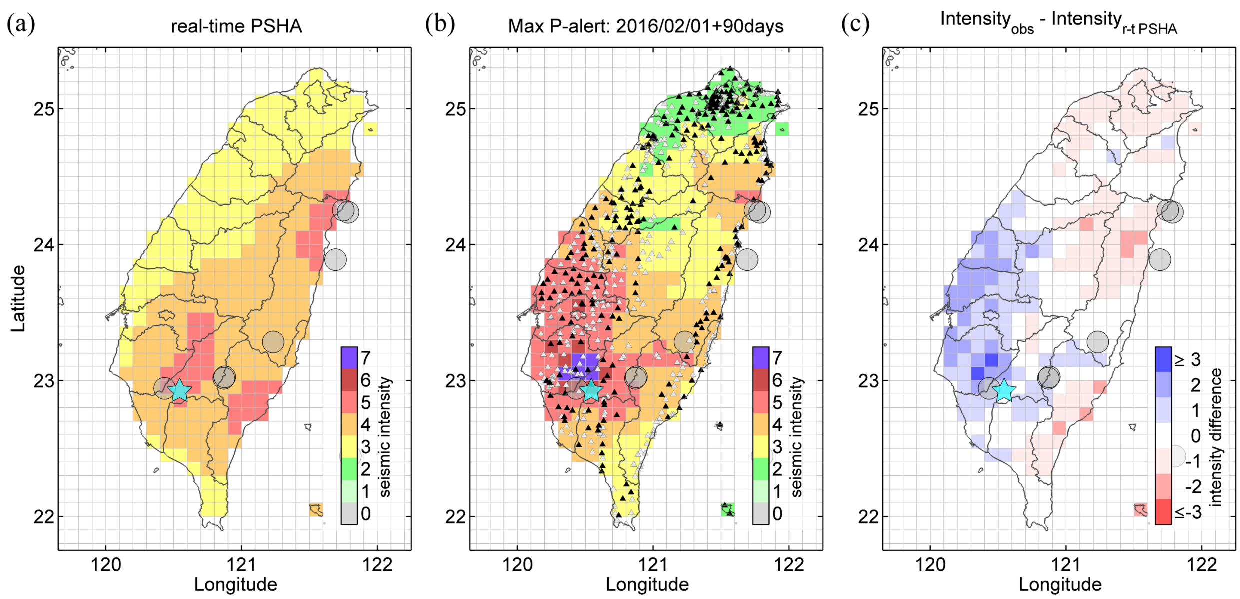

Figure 2. The case of 2016 Meinong earthquake: (a) The map of forecasting max seismic intensity by the rea-time PSHA. The forecasting interval of seismic intensity is 90 days. (b) The map of max seismic intensity recorded by the P-alert network. Black and white triangles indicate the P-alert stations which we used and didn't use in the verification, respectively. (c) The difference of seismic intensity between the forecast and the record. Cyan star represents the Meinong earthquake; gray circles represent the earthquakes with magnitude $M_L \geq 5$ in this forecasting interval.

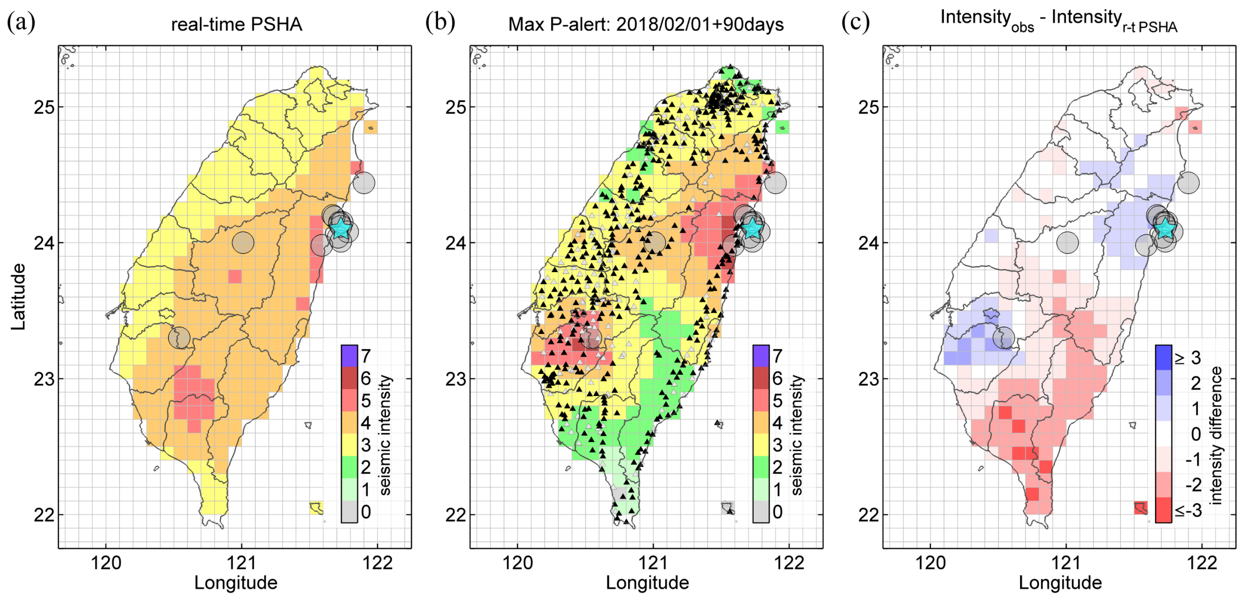

Figure 3. The case of 2018 Hualian earthquake: (a) The map of forecasting max seismic intensity. (b) The map of max seismic intensity recorded by the P-alert network. (c) The difference of seismic intensity between the forecast and the record. Cyan star represents the Hualian earthquake.

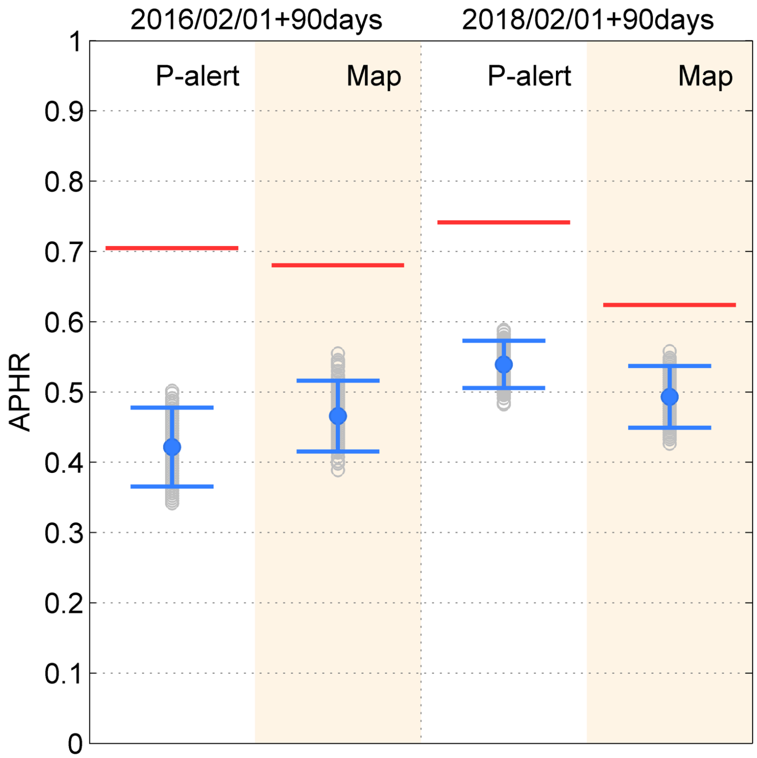

Figure 4. Performance test of APHR. Red line indicates the forecasts of the real-time PSHA; gray circle indicates the result of a random test by randomly re-distributing seismic intensities; blue error bar indicates the interval with two standard deviations over all random tests.

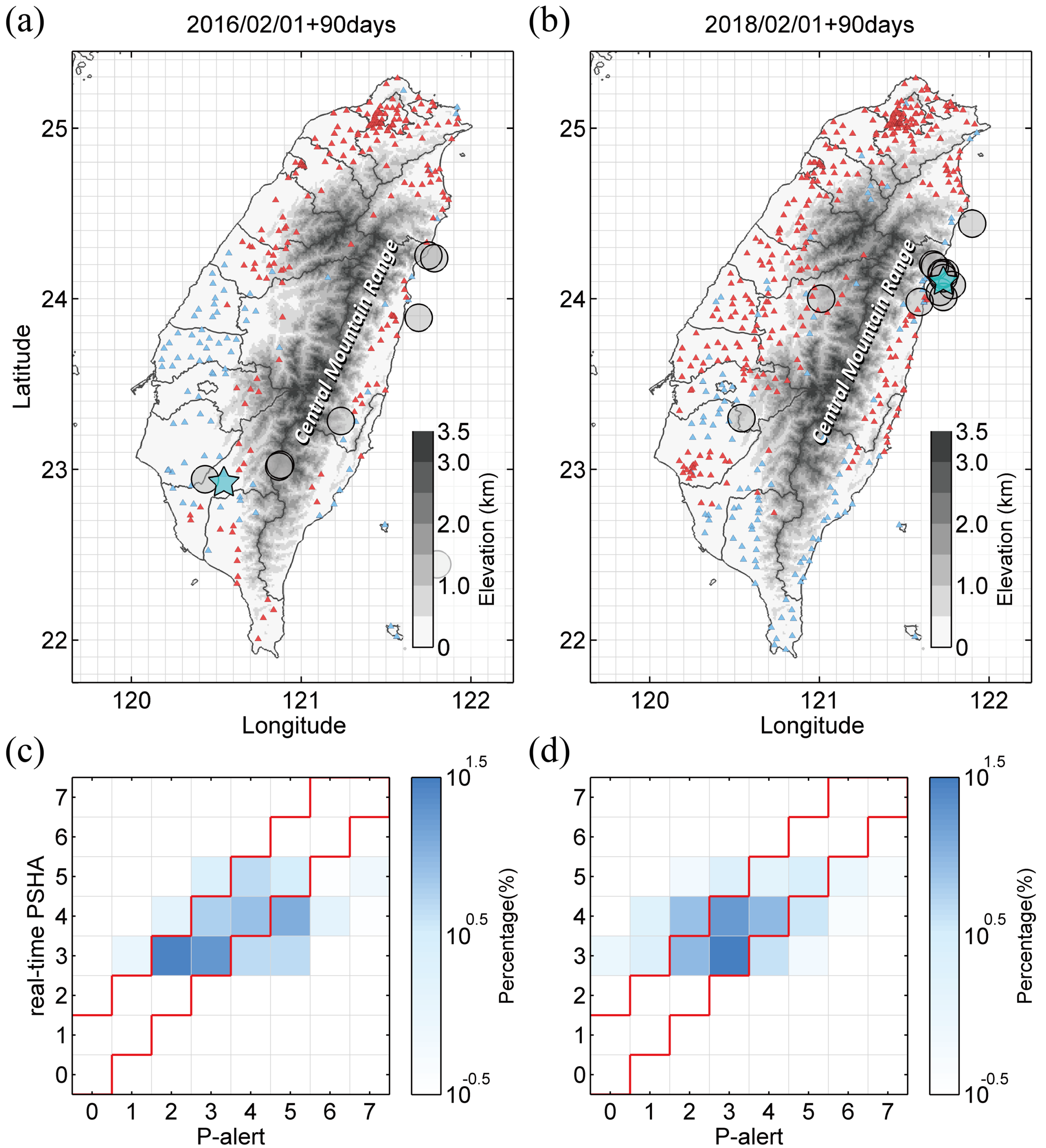

Figure 5. Panels (a) and (b) are the P-alert station distributions of the “hit” and “not hit”. Red and blue triangles present the “hit” and “not hit”, respectively. Panels (c) and (d) are the distributions of the hit percentage for the cases of 2016 Meinong and 2018 Hualian earthquake, respectively.

Red line area presents the acceptable prediction range.

Table 1. The earthquakes occurred in the forecast interval. “P-alert” indicates that the P-alert recording obtained from the Taiwan Earthquake Research Center (TEC) or the National Taiwan University (NTU). “Num.” is the number of recording stations. “Nan” indicates that there is no P-alert data to be recorded in both TEC and NTU even if that event was recorded by CWB. The bold represents the Meinong and Hualian earthquakes.

(a) Meinong case: 2016/02/01~2016/05/01

Date	Hour	Min.	Lon.	Lat.	Depth	M_{L}	P-alert	Num.
02/05	**19**	**57**	**120.54**	**22.92**	**14.64**	**6.60**	**TEC**	**338**
02/05	19	58	120.43	22.94	18.10	5.26	Nan	Nan
02/09	00	47	121.69	23.89	5.69	5.12	TEC	341
02/18	01	09	120.87	23.02	5.44	5.27	TEC	357
02/18	01	18	120.88	23.03	4.26	5.13	TEC	357
04/16	10	55	121.80	22.44	11.83	5.22	TEC	436
04/27	15	17	121.78	24.24	11.94	5.67	NTU	424
04/27	15	27	121.75	24.25	12.99	5.13	NTU	425
04/27	18	19	121.23	23.28	15.21	5.52	NTU	423

(b) Hualian case: 2018/02/01~2018/05/02

Date	Hour	Min.	Lon.	Lat.	Depth	M_{L}	P-alert	Num.
02/04	13	12	121.67	24.20	15.10	5.10	TEC	543
02/04	13	56	121.74	24.15	10.60	5.80	TEC	519
02/04	13	57	121.68	24.19	11.10	5.10	Nan	Nan
02/04	14	13	121.72	24.15	10.30	5.50	TEC	517
02/05	15	58	121.72	24.14	10.00	5.00	TEC	522
02/06	**15**	**50**	**121.73**	**24.10**	**6.30**	**6.20**	**TEC**	**520**
02/06	15	53	121.59	23.98	5.10	5.00	TEC	520

02/06	18	00	121.73	24.12	6.70	5.30	TEC	516
02/06	18	07	121.71	24.04	4.20	5.30	TEC	516
02/06	19	15	121.73	24.01	5.70	5.40	TEC	516
02/07	15	21	121.78	24.08	7.80	5.80	TEC	523
02/25	18	28	121.90	24.44	17.70	5.20	TEC	533
03/20	09	22	120.54	23.30	11.20	5.30	TEC	539
03/29	00	17	121.01	24.00	11.10	5.00	NTU	388
04/23	17	10	122.53	23.92	19.30	5.10	NTU	381

Table 2. The coefficients in the GMPE.

C_1	C_2	C_3	C_4	C_5	C_6	C_7	C_8	H
1.3979	0.3700	0.0000	-1.2273	0.2086	-0.1934	0.1122	-0.4359	1.4877

Table 3. Seismic intensity scale of CWB.

Intensity Scale		Ground Acceleration (cm/s^2, gal)
Micro	0	<0.8
Very minor	1	0.8~2.5
Minor	2	2.5~8.0
Light	3	8~25
Moderate	4	25~80
Strong	5	80~250
Very Strong	6	250~400
Great	7	≥400